Chem Soc Rev

TUTORIAL REVIEW

View Article Online
View Journal | View Issue

Cite this: *Chem. Soc. Rev.*, 2018, **47**, 7830

Computational chemistry strategies in natural product synthesis

Masha Elkin and Timothy R. Newhouse *

Received 1st May 2018

DOI: 10.1039/c8cs00351c

rsc.li/chem-soc-rev

The synthesis of natural products increasingly uses computational chemistry approaches to model and understand molecular phenomena. Calculations are employed to rationalize reaction outcomes, predict how a new system will perform, and inform synthetic design. As a result, new insights into the interactions of fundamental chemical forces have emerged that advance the field of complex small molecule synthesis. This review presents ten examples of computational techniques used in the synthesis of natural products, and discusses the unique perspectives afforded by these quantitative analyses.

Key learning points

(1) The computational methods that are used in support of multistep synthesis, including molecular mechanics, density functional theory, and non-covalent interaction analysis

(2) The types of systems that are suitable for computational modelling, including ground state, excited state, transition state, and transition state surrogate structures

(3) Strategies for simplifying calculations for practicality while maintaining accuracy

(4) How computational studies can rationalize reaction outcomes, including reactivity, regioselectivity, torquoselectivity, diastereoselectivity, and enantioselectivity

(5) How computational studies can inform substrate design and next-generation synthetic approaches

1. Introduction

1.1. Historical perspective and overview

Natural product synthesis is a field that has historically been rooted in detailed considerations of molecular structure. Such considerations include determining the composition of matter with challenges relating to bond connectivity, as in that posed by penicillin,[1] and elemental composition, as encountered in diazonamide.[2] Within the context of synthetic design and execution, structural factors that dictate chemical reactivity must be paramount for a total synthesis campaign to be successful. Above all, the consequences of reaction mechanism and thermodynamic parameters determine feasibility in multistep synthesis. Because of these inherent aspects of natural product synthesis, the tools provided by computational chemistry are easily adopted and present profound insights and opportunities.

The synergy of these fields began early in the 20th century, as researchers used approximations of quantum mechanical calculations to model molecular structures and rationalize experimental outcomes observed in synthetic studies.[3] This cooperation continues today, as reports of new synthetic accomplishments are increasingly accompanied by computational treatments.[4] As advances in computing power minimize the cost of its application, these studies become more prevalent and more accessible. While a typical transition state calculation decades ago would require months to run, the same calculation now takes seconds,[5] and many complex calculations can be performed on standard personal computers in addition to high performance computing resources. This tutorial review highlights several recent computational investigations supporting natural product synthesis with the goal of describing representative calculations that can be performed. We hope this review illustrates the modern power of computational chemistry when applied to natural product synthesis and leads to greater adoption of these methods by practitioners of multistep synthesis.

Computational techniques are poised to investigate various chemical properties by the careful selection of a computational method, given the computing resources available, the size of the system of study, the level of accuracy required, and other considerations.[4–6] Optimizing compound structures and calculating thermodynamic parameters such as enthalpy and free

Department of Chemistry, Yale University, 225 Prospect Street, New Haven, Connecticut 06520-8107, USA. E-mail: timothy.newhouse@yale.edu

energy enables the quantification of stability and is possible with molecular mechanics, *ab initio*, semi-empirical, and hybrid methods. Examination of structural features, charge density, and interaction energies can provide rationale for experimental trends by using non-covalent interaction and natural bond order analyses, among other techniques. Transition state energies offer kinetic information important for reaction mechanisms,[7] and transition state structures reveal molecular interactions that govern chemical outcomes. Importantly, computational techniques provide models that can be experimentally validated in order to support further extrapolations, although these must be accompanied by an understanding of the limitations and assumptions inherent in such models. The combination of these experimental and theoretical chemical subdisciplines is thus leveraged for greater understanding and application of underlying chemical forces.

1.2. Scope of this review

In the interest of space, we have narrowed the scope of this review to highlight variations of structure optimization as applied to natural product synthesis. This necessarily excludes reports that predict spectroscopic data for structure determination,[8] as well as studies that apply computational techniques to the development of synthetic methods,[9,10] biosynthetic studies,[11] or protein docking models.[12] These subjects will be mentioned only when in concert with calculations directly supporting natural product synthesis. Additionally, this work will not discuss the development of computer-assisted reaction design,[13] automated synthetic planning,[14,15] or other cheminformatic innovations. The advances in these fields are impressive and impactful, and readers are encouraged to examine these contributions through the many excellent reviews published on these topics.

This review highlights ten examples that showcase the use of computational studies in natural product synthesis. These examples are not comprehensive, and we regretfully acknowledge the volume of work that has been omitted due to space limitations. Our treatment of each example is by necessity limited, and readers are encouraged to examine primary sources. It is our hope that an overview of this work will highlight the unique contributions to chemical knowledge that computational techniques afford in complex synthetic settings.

2. Rational substrate design and predicting reactivity in natural product synthesis

The reasons behind the disparate reactivities of comparable substrates are often complex and varied. Computational insight can elucidate the underlying phenomena behind such observations and predict more reactive substrates for next-generation approaches towards synthetic challenges. The following sections identify conformational preferences responsible for reaction diastereoselectivity (Section 2.1), and substrate substitution that affects thermodynamic equilibria (Sections 2.2 and 2.3). Sections 2.4 and 2.5 investigate kinetically-controlled transformations through ground-state calculations, and Section 2.6 introduces transition state modelling for the rational design of a more reactive substrate.

2.1. Substrate conformation dictates diastereoselectivity

Molecular mechanics can complement qualitative analyses to predict reaction outcomes, as in the classic case of periplanone B (**4**, Scheme 1A). The total synthesis of **4** was first reported in 1979 by Still,[16] who correctly assigned the relative stereochemistry of the natural product by synthesizing several possible diastereomers. A key challenge in his approach consisted of accessing the correct diastereomer of the 1,2-disubstituted epoxide **3**. Still addressed this issue with a qualitative analysis of reactive conformers, which enabled the completion of **4**, and is complemented

Masha Elkin

Masha Elkin was born in Moscow and grew up in the greater Boston area. She received her BA in Chemistry from Washington University in St. Louis (2014), where she worked with Prof. Vladimir Birman on the development of amidine-based chiral ligands for transition metal catalysis. She is currently a graduate student with Prof. Timothy Newhouse at Yale University, where she works on natural product synthesis and synergistic computational studies.

Timothy R. Newhouse

Tim, a native of New Hampshire, received his undergraduate degree from Colby College (2005), where he was mentored by Prof. Dasan M. Thamattoor. He completed his PhD at The Scripps Research Institute with Prof. Phil S. Baran (2010) and during this time he also worked with Prof. Donna G. Blackmond. Subsequent postdoctoral studies were with Prof. E. J. Corey at Harvard University. He began his independent career at Yale University in 2013 and was promoted to Associate Professor in 2018. His research group develops chemical technologies and computational approaches for the step-efficient synthesis of natural products with potential applications to neuroscience.

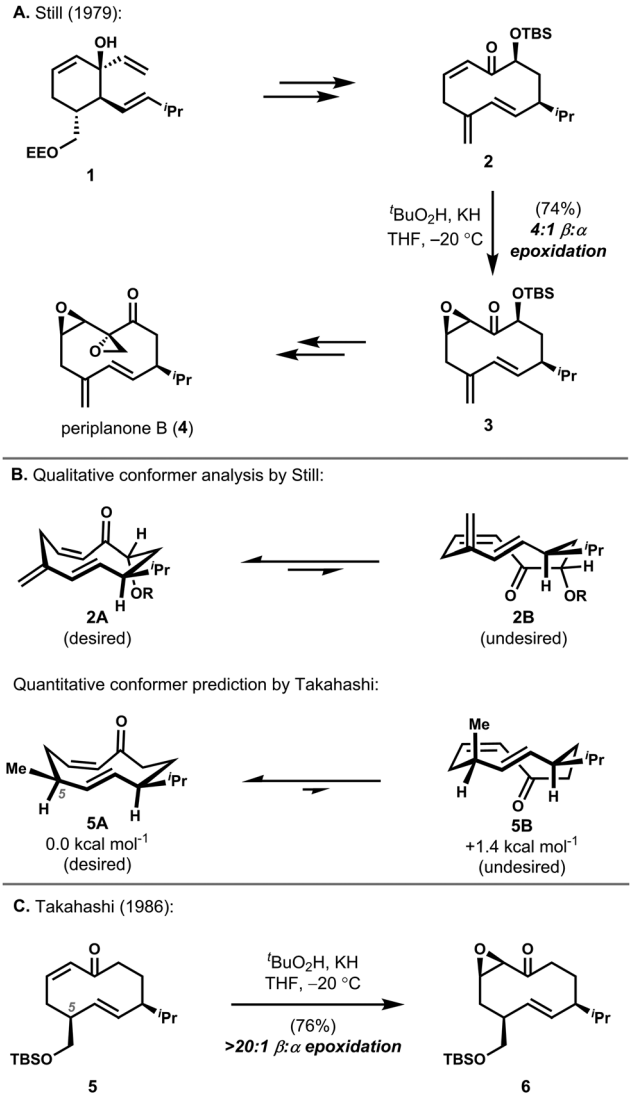

Scheme 1 (A) Still's synthesis of periplanone B (**4**). (B) Conformational analysis by qualitative and quantitative methods. (C) Takahashi's approach to **4**.

in this work by Takahashi's later computational treatment of a similar epoxidation.[17] Given the synergy of these qualitative and quantitative approaches for the epoxidation towards **4**, which is representative of a typical synthetic and computational workflow, both studies are discussed here.

In his approach, Still established the peripheral model of attack,[18] a theoretical approach for predicting the diastereoselectivity of reactions on medium-sized rings. The axiom states that reagents will approach from the outside of a ring in its lowest energy ground state conformation. Still used this insight to design a substrate for alkene epoxidation that underwent β-selective epoxidation for a route towards **4**. Still elaborated **1** to diene **2**, reasoning that steric preference for the s-*trans* conformer **2A** over s-*cis* **2B** would favour the configuration leading to β-epoxidation (Scheme 1B). His hypothesis was supported empirically; epoxidation occurred with 4 : 1 selectivity for β-epoxidation, enabling the completion of the first synthesis of periplanone B (**4**), the assignment of the correct relative stereochemistry, and the provision of material to correctly assign the absolute stereochemistry.

While Still used qualitative analysis to intuit low-energy substrate conformations to predict diastereoselective alkene epoxidation, in 1986 Takahashi and co-workers used molecular mechanics (MM) to quantitatively predict the outcome of a similar epoxidation event.[17] In their approach, the ten-membered ring epoxidation substrate **5** was accessed by intramolecular alkylation (Scheme 1C). MM2-calculated conformers of **5** (CH_2OTBS abbreviated as CH_3) are shown in Scheme 1B (**5A** and **5B**). Lowest energy structures display a *syn* relationship between the enone carbonyl and C5 β-methyl group to minimize transannular strain, as in **5A**. Based on the five lowest energy conformers of **5**, the authors predicted a 92% population of conformers leading to β-epoxidation at room temperature. When subjected to Still's epoxidation conditions, the authors in fact observed exclusive formation of the desired β-epoxide (**6**). They were able to elaborate this intermediate to periplanone B (**4**) in short order.

Through these efforts, Takahashi and co-workers predicted that the inclusion of a C5 β-alkyl group to a periplanone-like intermediate would induce conformational preferences favouring β-epoxidation. Their approach built on the work of Still and others and was informed by MM2 structure predictions which indicated that methyl substitution at C5 introduces transannular strain when disposed *anti* to the enone carbonyl. These insights demonstrate that subtle changes in the substitution of medium-sized rings can result in dramatic conformer rigidity. The hybridization and stereochemistry of a single position in a ring may bias a compound to a dominant conformation.

The study of periplanone B (**4**) clarifies how molecular mechanics can complement qualitative analysis. Although the exclusive use of MM calculations has generated landmark studies for decades, modern technology has enabled more nuanced density functional theory (DFT) calculations to be run even on personal computers. A DFT single point energy calculation following a MM structure optimization is within the technological capabilities of most synthetic researchers. Such studies are limited to systems which are adequately described by the MM parameters. In contexts where the energetics of systems with multiple degrees of freedom are challenging to intuit, computational chemistry can be an important tool for evaluating and predicting trends and properties. Computational chemistry can be especially instructive when competing factors complicate qualitative analysis.

2.2. Mapping the reactivity of diastereomeric substrates

Calculations can explain and predict the disparate reactivities of diastereomeric substrates under the same reaction conditions. This is exemplified by the synthesis of a number of dioxabicyclic bromoallene natural products including isollaurallene (**7**), laurallene (**8**), and related compounds, as reported by Kim and co-workers in 2012 (Scheme 2A).[19] The authors accomplished these syntheses by substrate-controlled diastereoselective alkylation strategies and a key ring-closing metathesis (RCM) with

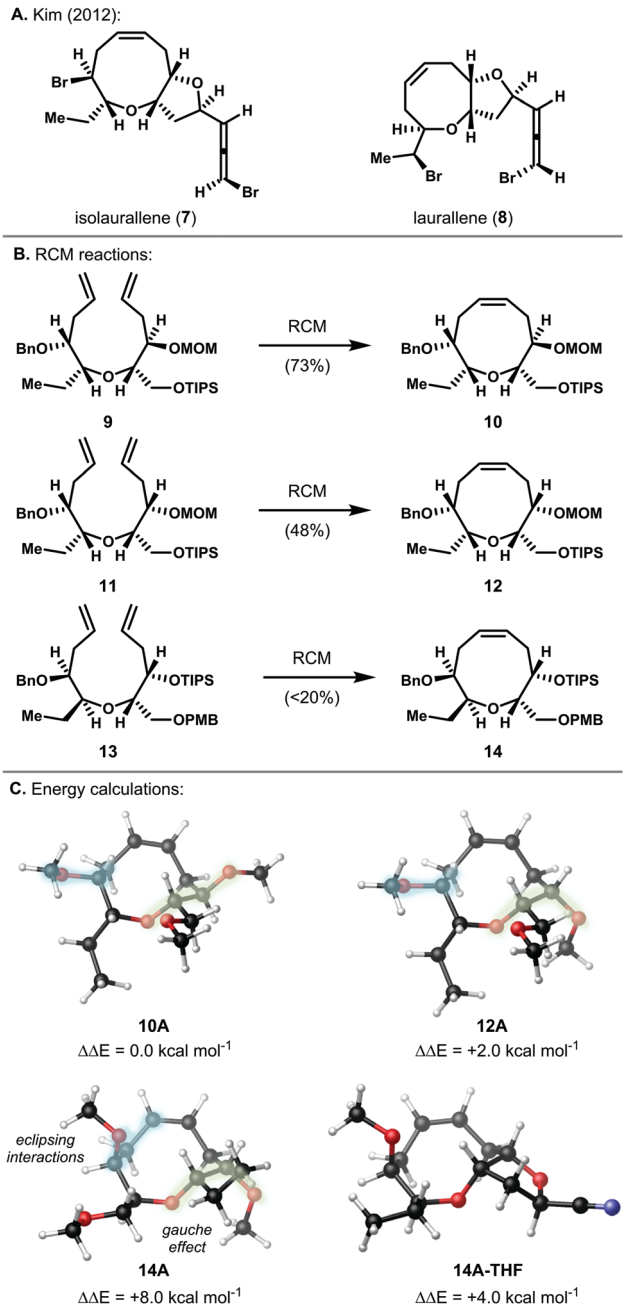

Scheme 2 (A) Natural products targeted by Kim and co-workers. (B) Relative reactivities of diastereomeric substrates, with reaction conversion indicated in parentheses. (C) Relative MMFF energies of RCM reactions and optimized product structures.

Grubbs' second generation catalyst to form the medium-sized cyclic ether. It was found that the success of the RCM depended heavily on the substitution pattern of the substrate. Substrate **9** (Scheme 2B) underwent smooth RCM (73% conversion) while the diastereomeric **11** did so with depreciated conversion (48%). A different diastereomer, **13**, did not undergo RCM efficiently (<20%). Intrigued by this and desiring a variety of diastereomeric products to access various bromoallene natural products, the authors modelled eight diastereomers of the substrate **9**, with protecting groups abbreviated as CH_3 to reduce computational cost, and investigated the extent of RCM *in silico*.

The authors performed a 10 000 step Monte Carlo conformational search to explore many conformers of the relatively flexible substrates and products, followed by MMFF or OPLSAA force-field energy minimizations (MMFF reproduced here, Scheme 2C). The authors calculated energies for the uncyclized starting materials and cyclized products to compare $\Delta\Delta E$ values, the relative thermodynamic favourability of reactions to occur. Modelling the reaction transition states or Ru-complexed substrates and products was computationally intractable due to the conformational flexibility and complex mechanistic possibilities of these systems, and thus was not pursued. Simplified thermodynamic parameters are often sufficient to explain observed trends due to thermodynamic control in reversible reactions; this simplified analysis makes calculations faster and easier to perform. The authors found the energies of the starting materials to be nearly equivalent (all within 0.5 kcal mol^{-1}) due to the conformational flexibility of the open-chain form. The products do not benefit from the same advantage and differ significantly in energy. This difference comprises the overall thermodynamic preference for the formation of certain oxacyclononenes. The trends revealed by comparing reaction $\Delta\Delta E$ values, which depend on relative product stability, agree with empirical results and reveal important factors in the stability of oxacyclononene rings.

Lowest energy conformers of **10A**, **12A**, and **14A** are shown in Scheme 2C. These diastereomers were found to exist in an asymmetric conformation with respect to the 9-membered ring. The product **10A** is most stable, corresponding to the RCM of greatest conversion (**9** → **10**, 73% conversion). Diastereomer **12A** is 2.0 kcal mol^{-1} less stable than **10A**, and corresponds to the product **12**, which was formed in 48% conversion. The least stable conformer (**14A**) was formed in <20% conversion. An analog of **14A** in which the tetrahydrofuran moiety of the natural product was introduced (**14A-THF**), pre-organizing the substrate towards RCM, was predicted to be 4.0 kcal mol^{-1} more stable than **14A**. Indeed, this analog underwent cyclization in 57% yield under slightly modified reaction conditions, and was used by the authors for the synthesis of itomanallene A.[20] The calculated trends were consistent with empirical data, thus validating the extrapolations provided by the model.

The reasons for the disparate stability of the diastereomeric products were investigated. Inspection of the structures revealed that destabilizing eclipsing interactions contribute to the energetic differences. In the most destabilized conformer **14A**, the methoxy group partially eclipses the carbon backbone of the cyclic ether (blue highlight, left), which is a more penalizing interaction than the analogous eclipsing interaction between the methoxy group and a C–H bond found in **10A** and **12A**. To mitigate this interaction, a stabilizing *gauche* configuration between the vicinal ethereal C–O bonds is present in **14A** (green highlight, right).[21] The *gauche* effect occurs when the *gauche* rotamer of a compound is more stable than the corresponding *anti* conformer, and is explained in part by stabilizing hyperconjugative interactions with the polarized

bond (in this case, $\sigma_{CH} \rightarrow \sigma^*_{CO}$). However, the most stable conformer **10A** lacks this stabilizing *gauche* interaction and instead assumes an antiperiplanar relationship between the ethereal bonds, thus minimizing torsional strain at the expense of the *gauche* effect stabilization. This implies that stereoelectronic effects are less consequential than steric interactions in this system, and that the net effect of these competing factors can be predicted by computational means.

The authors were able to leverage the reactivities of RCM substrates to the successful syntheses of numerous dioxabicyclic bromoallene natural products. Recognizing that the RCM **11** → **12** was limited to 48% conversion, they pre-formed the tetrahydrofuran ring and were then able to perform the RCM (**11-THF** → **12-THF**, not shown) in 96% yield. The authors used this and other RCM adducts to access **7**, **8**, and other natural products. In doing so, they contributed insights into competitive stabilizing interactions, such as the limitations of the *gauche* effect and nuances as to the conformational preference of oxacyclononenes.

One of the key features of this study is that reaction thermodynamics can be used in place of modelling exact reaction conditions, including challenging calculations of metal complexes. This is appropriate when considering thermodynamic equilibria, or cases where the Hammond postulate can be applied to relate transition state energies to ground-state structures, but such approximations must be carefully considered. While a powerful and necessary tool to reduce computational cost to manageable levels, reaction and substrate simplification can skew predicted results when steric or conformational effects are not accurately reflected by the truncated system. Although some systems cannot be simplified while maintaining accuracy and relevance to the experimental study, many systems can be truncated effectively, especially in the relatively small and rigid systems described in this tutorial review. By prioritizing such carefully considered economic calculations, computational techniques can efficiently complement synthetic studies.

2.3. Relative product energies predict reaction outcomes

Thermodynamic equilibria can beguile synthetic researchers but become elucidated by computational treatment. An excellent example is the 2012 report from the Evans group on synthetic studies towards numerous GB alkaloids.[22] In the construction of *ent*-himgaline (*ent*-**18**) and *ent*-GB 13 (*ent*-**17**), shown (along with synthetic intermediates) as enantiomers in Scheme 3A for ease of comparison with Scheme 3B, an enamine aldol cyclization was used as a key bond construction reaction. Diketone *ent*-**15** reacted to form *ent*-**16** with full cyclization and was progressed to *ent*-GB 13 (*ent*-**17**) and *ent*-himgaline (*ent*-**18**). The authors then targeted the related alkaloid himandrine by a similar enamine aldol cyclization, but found that their original aldol conditions (HOAc, THF) on an analogous substrate did not result in cyclization (**19** → **20**, Scheme 3B). The cyclization precursor **19**, although structurally similar to **15**, was found to undergo spontaneous cyclization only under neutral conditions in polar protic solvents such as methanol. Additionally, several analogs of **15** and **19**, such as **21**, were investigated for cyclization and found to be unreactive under any conditions. It was found that the reversibility of the cyclization precluded full conversion to product. To better understand the thermodynamics of the system and the reason for such high substrate specificity, the authors employed computational modelling.[22,23]

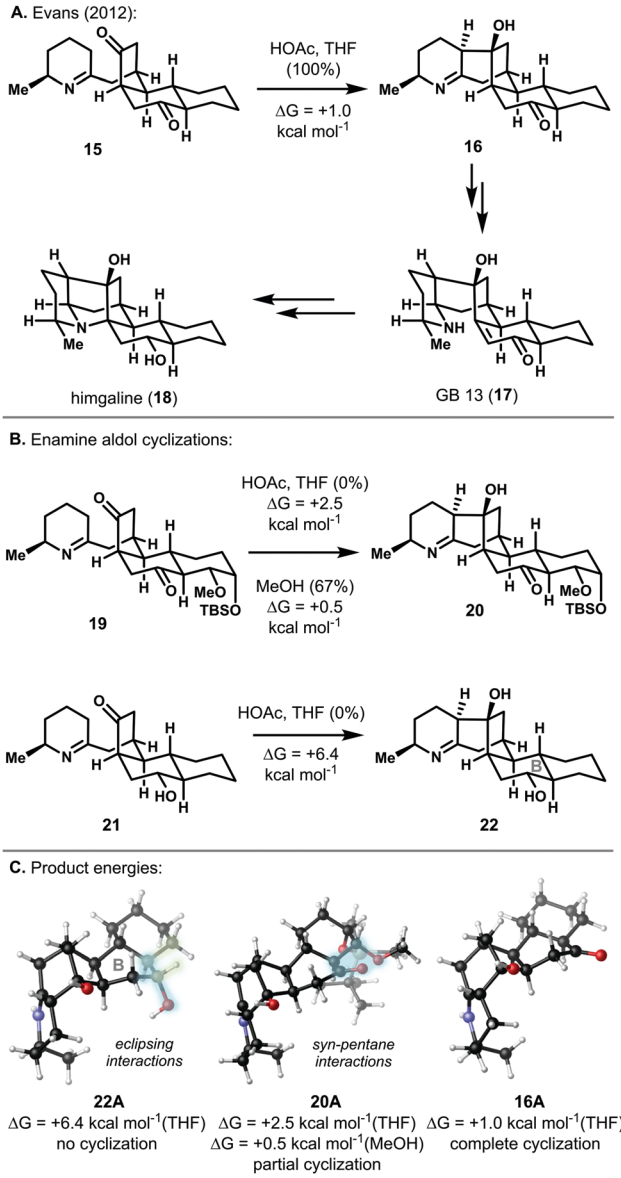

Scheme 3 (A) Syntheses of *ent*-**17** and *ent*-**18** by enamine aldol cyclization, shown as enantiomers for clarity, with reaction conversion indicated in parentheses. (B) Aldol cyclizations of less reactive systems, with reaction conversion indicated in parentheses. (C) Computed product energies, energy-minimized structures, and destabilizing interactions.

The authors performed Monte Carlo conformational searching followed by DFT structure optimization at different levels of theory, with M06-2X/6-31G(d) results reproduced here. They first investigated model aldol reactions. The dimerization of acetone was found to be thermodynamically similar whether enamine- or enol-mediated. The transformation is enthalpically favoured, but entropically disfavoured by *ca.* 12 kcal mol^{-1},[24] resulting in an overall endothermic reaction favouring the

starting materials by 5–10 kcal mol^{-1}. The intramolecular aldol the authors pursue in their synthetic route benefits from lacking an entropic penalty, thus requiring further investigation of the reaction enthalpies in this complex system to account for low reactivity.

The authors modelled the enamine aldol cyclizations in systems for which they had empirical data. The cyclization used in the synthesis of *ent*-himgaline (*ent*-**18**) and *ent*-GB 13 (*ent*-**17**) was predicted to be endothermic by 1.0 kcal mol^{-1} (**15** → **16**). The cyclization **19** → **20** towards himandrine, which was unreactive under the same reaction conditions, is endothermic with ΔG = +2.5 kcal mol^{-1}. These systems included *N*-protonated intermediates because of the acidic reaction conditions, but when the neutral reaction of **19** in methanol (SMD solvation model) was investigated, a more favourable ΔG = +0.5 kcal mol^{-1} was predicted. This is consistent with experimental results, in which only neutral conditions led to product formation for this substrate. Although reaction energies are overestimated in every case, the relative free energy values trend with reactivity. Small discrepancies between predicted and observed reactivities may be due to the limitations of implicit solvation methods, which do not account for hydrogen-bonding and other significant effects.[25,26] Finally, alcohol **21** and an unsaturated derivative (not shown) did not cyclize to any extent under neutral or acidic conditions, and the free energies for these transformations were calculated to be +6.4 and +3.3 kcal mol^{-1}, respectively, under acidic conditions. This is intriguing because these structures are very similar to successful substrates **15** and **19**, and the differences in substitution are remote from the site of bond construction. The difference in reactivity between **15** and **19** is also notable for this reason. A more detailed look at conformational preferences was necessary to explain this phenomenon.

The starting materials for the aldol cyclizations were found to be similar in energy, so the product structures were investigated in more detail (Scheme 3C). While the decalin framework in the starting materials adopts a chair–chair conformation, the cyclized products were found to be most stable in a B-ring boat conformer in a model system calculation, where the B-ring chair conformer is more unstable by 3.7 kcal mol^{-1}. The intermediates in Evans' study adopt this conformation, and the steric interactions imposed by this constraint explain reactivity. For example, when the carbonyl was reduced as in **22A**, the subsequent sp^3 carbon orients such that eclipsing interactions are introduced (blue and green highlights). This substrate is 6.4 kcal mol^{-1} disfavoured from cyclizing as a result of these interactions, and no cyclization was observed experimentally. This is not the case in the more stable **16A**, which formed with full conversion. Cyclization product **20A**, which formed with 67% conversion, experiences a *syn*-pentane interaction between the carbonyl and methoxy groups (blue highlight). These observations explain the different reactivities predicted by calculations and observed by the authors experimentally.

Calculations in this case were used to map a reversible process and explain where equilibria lie in a series of related systems. The reactivity was explained by computing model systems which identified underlying energetic preferences, and by using these insights to identify destabilizing interactions in the real systems. For example, conformational restrictions on the bicyclic system—a B-ring boat conformation, as predicted by a model—implicated destabilizing interactions in substrates that agreed with experimental cyclization rates. While the predicted and experimental trends in reactivity were in agreement, absolute energy values were systematically skewed because of the difficulty of accurately modelling solvent effects using implicit solvation methods.[25,26] These insights and techniques may be applied more broadly to the use of model systems in computational studies, to our understanding of reaction equilibria, and to our appreciation of the influence of remote substitution on substrate reactivity.

2.4. Kinetic control: the Hammond postulate enables the use of ground state structures to explain reactivity

Ground state calculations can be used to model both reversible, thermodynamically-controlled and irreversible, kinetically-controlled transformations because the Hammond postulate relates transition state structures and energies to neighboring intermediate structures and energies. This simplifies computational cost, as in Stephenson's instructive syntheses of (+)-coronaridine (**25**), (−)-pseudotabersonine (**26**), and (−)-pseudovincadifformine (**27**, Scheme 4A).[27] In this 2014 study on catharanthine alkaloids,

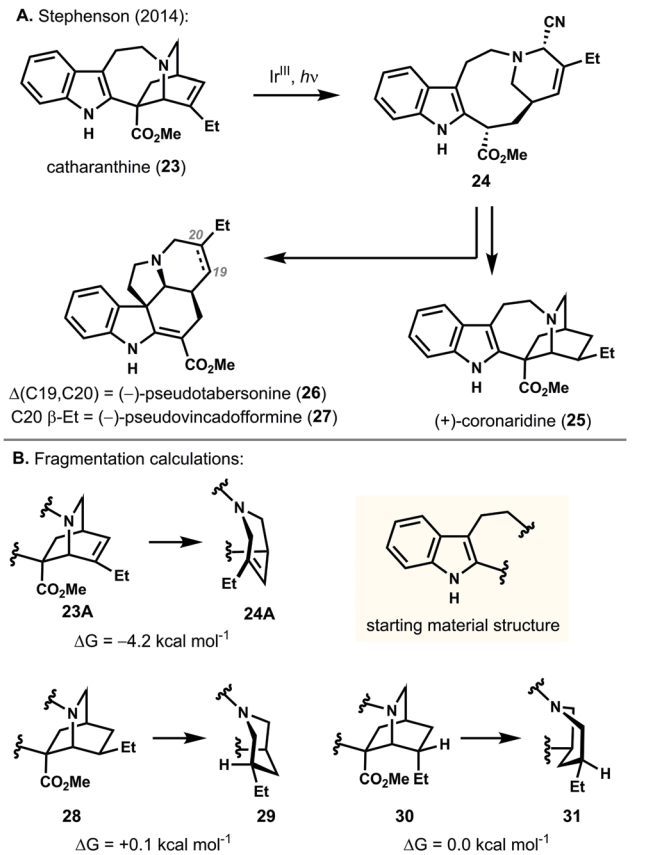

Scheme 4 (A) Synthesis of natural products through fragmentation of catharanthine (**23**). (B) Relative fragmentation energies of systems explored by Stephenson and co-workers.

strain release is identified as a major driving force in a critical photoredox reaction.[28] The photoredox-induced fragmentation of **23** with $Ir(dF(CF_3)ppy)_2(dtbbpy)PF_6$, visible light, and trimethylsilyl cyanide occurred in good yield and with high stereoretention to form **24**. This intermediate was elaborated to a number of alkaloid natural products, including **25**, **26**, and **27**. In investigating the generality of this transformation to similar ring systems, the authors identified a key reliance on strain as a driving force; while **23** undergoes fragmentation with high efficiency, saturated analogs **28** and **30** suffer decreased yields of fragmentation (Scheme 4B). DFT calculations (B3LYP/6-31G(d)) elaborated on these findings.

Energy-minimized structures of azabicyclo[2.2.1]octanes **28** and **30**, and unsaturated **23A** were compared to those of fragmentation products **29**, **31**, and **24A**, respectively, to investigate the ring strain associated in each system. Cleavage for **23A** is 4.2 kcal mol^{-1} downhill in energy, while the saturated analogs **28** and **30** are energetically neutral and fragmented in only 25% and 37% yield, respectively. The strained alkene **23A** is responsible for the release of energy during this transformation, a driving force missing in **28** and **30**. This comparison allows a rough assignment of 4.2 kcal mol^{-1} for the strain energy introduced in an azabicyclo[2.2.2]octane by a bridging olefin.[29] Strain release and fragmentation approaches have been favoured strategies in complex synthesis,[30] so these results have direct application both for these specific systems and as a greater approach towards the quantification of fragmentation energy.[31]

While **28** and **30** lack the ring strain of a bridging olefin, they are not energetically equivalent. The axially-disposed ethyl moiety in **30** introduces significant 1,3-diaxial strain to the system, such that **28** is more stable than **30** by 3.2 kcal mol^{-1}. However, this destabilizing interaction in the starting material is balanced by another in the product, so the overall reaction is energetically neutral. The product **31** adopts a boat conformation to avoid steric interactions between the ethyl and amine substituents, and thus incurs an energetic penalty that matches the 1,3-diaxial strain in **30**.

Through these studies the authors use visual inspection of predicted ground state structures and relative energies to rationalize experimental results and trends. A key advantage of this approach is the relative low computational cost and ease of locating lowest energy ground states, thereby avoiding more intensive transition state calculations. This is possible because of the relationship between ground state and transition state structures and energies asserted by the Hammond postulate. This approach must be used with caution because there are several exceptions to the Hammond postulate,[32] such as Curtin–Hammett scenarios wherein relative transition state energies are solely responsible for product formation. However, Stephenson's study is a template for using ground state energies to understand irreversible reactions and complex reactivity in natural product synthesis, and is an example of how strain energy can be understood at a high level of detail to explain chemical reactivity. The authors' use of B3LYP/6-31G(d) represents a popular choice of practitioners for a generally accurate and economic computational method, that has seen recent improvements through the inclusion of dispersion forces.[33–35]

2.5. Ground state calculations as surrogates for reaction transition states

Application of the Hammond postulate enabled Baran and co-workers to calculate the relative energies of several taxane radicals as a proxy for transition state energies, to predict the site of reaction with diverse electrophilic oxidants.[36] In their landmark 2014 elaboration of taxadiene (**32**) to taxuyunnanine D (**33**), the iterative allylic oxidations at C5, C13, and C10 were reported (Scheme 5A).[37] While the regioselectivity of allylic oxidation can sometimes be inferred qualitatively, a quantitative understanding is often more instructive and useful to synthetic researchers.

The authors calculated the most stable carbon-centered radicals in taxadiene-type systems to predict the regioselectivity of allylic oxidation for different substrates. The favoured site of allylic oxidation for **34–36** are indicated with arrows in Scheme 5B. DFT calculations (UB3LYP/6-31+G(d,p)) were used to compute the relative energies of radical species as a measure of the site of oxidation. It was found that substitution about the tetrasubstituted olefin greatly influenced the stability of proximal radicals. For **34**, the most stable radical was found to be the secondary position on the six-membered ring (C13). Despite the greater oxidation potential of 8-membered rings as compared to 6-membered rings due to the release of ring strain during oxidation,[38] the bicyclic nature of the 8-membered ring in **34** greatly disfavours this position towards oxidation. The 6-membered ring secondary radical was calculated to be more stable by 10.6 kcal mol^{-1}. Additionally, the primary radical formed by oxidation at the vinylic methyl position (C18) was

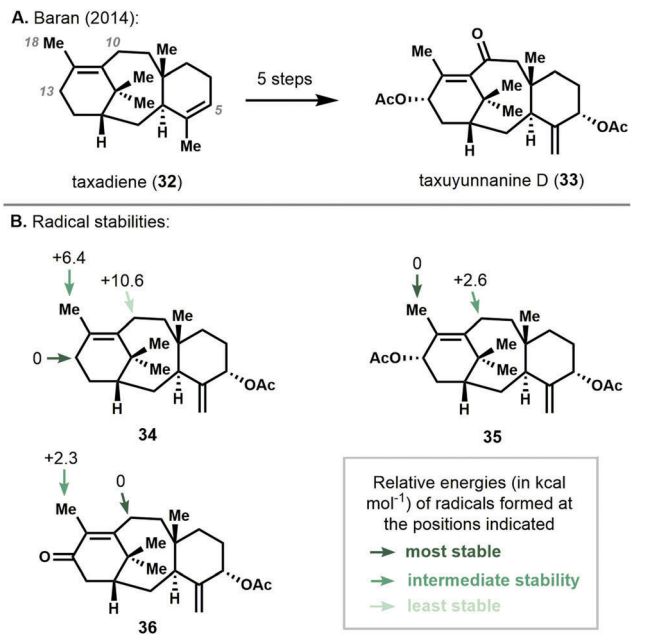

Scheme 5 (A) Elaboration of **32** to **33** through iterative oxidations. (B) Relative energies of allylic radicals within substrates.

predicted to be 6.4 kcal mol^{-1} less stable than that at C13. This result is supported empirically, wherein chromium-mediated oxidation resulted in allylic substitution of **34** at C13.[37,39]

The nature of the oxidation state at C13 determines the site of subsequent oxidation. If this position bears an acetoxy group as in **35**, the C18 radical was predicted to be more stable than that at C10 by 2.6 kcal mol^{-1}. This is in contrast to the case of the more highly oxidized compound **36** that possesses an enone rather than an allylic ester at C13. In this case the more stable radical is not the one formed at the methyl group but instead at the methylene of the 8-membered ring, C10, by 2.3 kcal mol^{-1}. This reversal in selectivity is presumably due to the greater stabilization afforded to the conjugated radical at the γ-position of the enone, rather than the cross-conjugated system for a radical formed at the methyl group.[40] Calculations enable researchers to account for these factors and make predictions that support and inform synthetic efforts. The site-selectivity predicted by Baran and co-workers was borne out empirically; allylic oxidation of enone **36** with *N*-bromosuccinimide occurred at the secondary position without competitive methyl oxidation. These efforts allowed the authors to introduce oxidation in taxadiene (**32**) iteratively at C5, C13, and C10, to complete the synthesis of taxuyunnanine D (**33**).

For instances where different reagents may be used that proceed by a variety of mechanisms, modelling generic intermediates as a substitute for multiple complex transition states is an enabling way to use computational chemistry in natural product synthesis. The precise modelling of various allylic oxidation methods is computationally difficult because of the large number of potential mechanisms and competent oxidants present in reactions mixtures. In this particular case, the energies of radicals predicted the site of allylic oxidation because the build-up of charge deficiency in the transition states for various allylic oxidations resembles that of the radical species. The use of ground state structures as transition state surrogates is thus most applicable when supported by mechanistic rationale. The energy and geometry of high-energy species can often be extrapolated to neighbouring transition states, as per the Hammond postulate.

2.6. Transition state modelling informs substrate design

Strategic syntheses often include second-generation substrate design, which can be guided by computational insights. In 2018 the Overman group reported a remarkable synthesis of (−)-chromodorolide B (**40**) *via* a strategic radical cyclization cascade (Scheme 6A).[41] By initiating the radical cleavage of redox-active ester **37** with $[Ru(bpy)_3](PF_6)_2$, Hantzsch ester, and blue light LEDs, the authors were able to observe 1,4-addition to (*R*)-5-methoxybutenolide to form **38**. This intermediate underwent 5-*exo*-trig cyclization and C–Cl cleavage to form **39**, which was elaborated to (−)-chromodorolide B (**40**). The yield for the overall reaction was low due to competitive quenching of **38** and nonselective 5-*exo* cyclization that favoured the undesired diastereomer at C8. Computational methods were employed to elucidate the mechanism of this transformation, rationalize the observed diastereoselectivity, and identify avenues for reaction optimization.

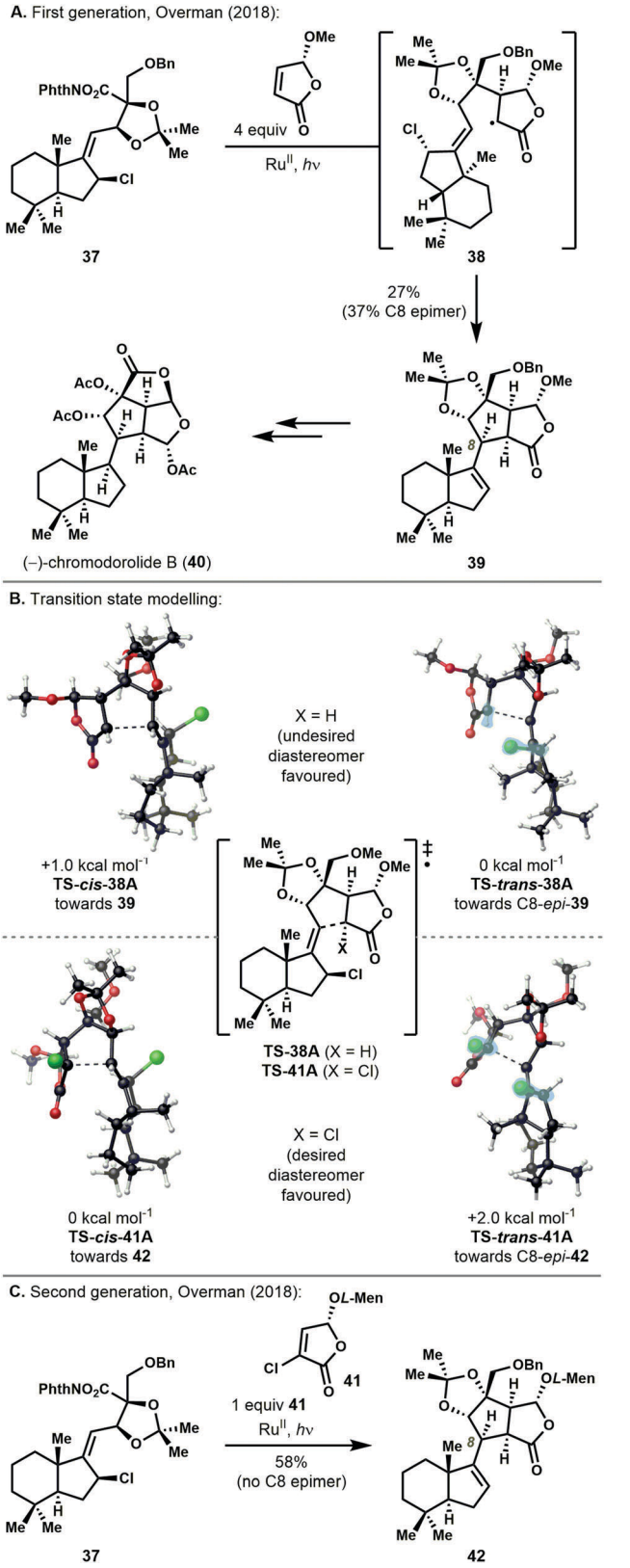

Scheme 6 (A) First-generation approach to (−)-chromodorolide B (**40**). (B) Computations suggest a new substrate design. (C) Second-generation approach to **40**.

For these studies the authors employed DFT methods for energy minimization (TPSS/def2-TZVP with BJ-damped D3-dispersion)[34,35] and single point calculation (TPPSh/def2-TZVP) (Scheme 6B). Energies in dichloromethane and acetonitrile were calculated by the COSMO model to account for solvent effects, with dichloromethane values reproduced here. Starting from abbreviated structure **38A** (see **38**, OBn abbreviated as OMe), the 5-*exo* cyclization was modelled to investigate the mechanism of this transformation. It was hypothesized that the lactone α-radical could undergo direct 5-*exo* cyclization with the pendent alkene, or reduction to the lactone enolate and an S_N2' reaction with the allylic chloride. Both transformations were modelled and found to be thermodynamically and kinetically accessible. Preference for one mechanism was ascertained by predicting the distribution of diastereomers and comparing that to the empirical distribution. The radical mechanism predicted a 0.5 kcal mol^{-1} energy difference in the cyclization transition states, corresponding to a desired : undesired product ratio of 1 : 2.5. The anionic mechanism reversed this trend, favouring the desired diastereomer by 0.7 kcal mol^{-1}, a 3.4 : 1 distribution. The observed product distribution of 1 : 1.3 favouring the undesired product is more consistent with the radical mechanism.

Shown in Scheme 6B are cyclization transition states with *cis* and *trans* configurations of the chlorohydrindane and lactone that lead to the desired and undesired products, respectively. When X = H, **TS-*trans*-38A** was predicted to be more stable by 1.0 kcal mol^{-1}, a bias the authors intended to reverse. Reasoning that the *trans* conformer could be disfavoured by introducing penalizing steric interactions, the authors targeted the lactone α-position for substitution. The introduction of a chlorine atom at this position (X = Cl, **TS-41A**) induces steric clash in **TS-*trans*-41A** (blue highlight) that is avoided in the *cis* conformer. This stabilizes the *cis* conformer by 2.0 kcal mol^{-1} and favours the desired product. The inclusion of a chlorine at this position was also predicted to decrease the bond-forming distances and shift the transition state geometry towards a later transition state, further enforcing the steric considerations favouring **42**.

These predicted results were validated by experimental findings (Scheme 6C). The 3-chlorobutenolide **41** was prepared and coupled to acetonide **37**. The substituted butenolide effected a doubling of the yield of the desired transformation and the undesired diastereomer was not detected. The authors were also able to decrease the equivalents of the butenolide fragment to equimolar amounts with **37**, and the reaction proceeded with organocatalysts in addition to precious-metal photoredox catalysts. The authors advanced this material for a more efficient synthesis of **40**.

Through these studies, the authors clarified the mechanism of a key cyclization reaction.[7,41] They built a computational model that was vetted with empirical data and used to predict the reactivity of new substrates. They also included dispersion forces in their calculations, which are increasingly recognized as crucial for attaining accurate energy values.[34,35] Visual inspection of transition state structures enabled the authors to identify potential sites to introduce steric interactions. In doing so, they selectively impeded the undesired reaction pathway and greatly improved the yield of their transformation. While this approach has the potential to positively change the desired transition state, it may also introduce an alternative reaction mechanism or otherwise invalidate the desired transition state structure; this technique is thus best used in a relatively rigid and mechanistically constrained system and with recognition of these potential problems. The Overman group successfully implemented this approach to enable substantial improvements to their synthetic route. This ability to see potential, not just existing, steric and electronic interactions is a key computational tool that synthetic chemists can use to propel their studies.

3. Asymmetry in synthesis explained through calculations

Computational techniques are adept at explaining the asymmetry induced in reactions, by modelling one substrate undergoing competing reaction pathways.[33,42] The examples in this section discuss reaction coordinate mapping and transition state inspection to rationalize diastereoselectivity (Sections 3.1 and 3.2) and enantioselectivity (Section 3.3). Applications to biosynthetic studies (Section 3.2)[11] and methods development (Section 3.3)[9,10] are discussed as well.

3.1. Rationalizing torquoselectivity with chair-like transition states

Ellman and Houk analysed the diastereoselectivity of a key electrocyclization reaction in an exceptional synthesis of an opioid small molecule,[43] wherein calculations clarified the energetic preference for a 6-membered ring chair-like transition state. This electrocyclization was a key step in a Rh(I)-catalysed reaction cascade for the synthesis of *ent*-ketorfanol (**46**, Scheme 7A). The diastereoselectivity of this transformation was crucial for the successful synthesis and depended on the torquoselectivity of the disrotatory electrocyclization. Treatment of **43** with catalytic $[RhCl(coe)_2]_2$ and 4-(diethylphosphino)-*N*,*N*-dimethylaniline as ligand in toluene at 55 °C effected alkyne hydroalkenylation to **44** and 6π electrocyclization to form a dihydropyridine. *In situ* reduction with $NaHB(OAc)_3$ afforded **45** in 69% yield and >20 : 1 dr; this product was elaborated to *ent*-ketorfanol (**46**) in short order. It was found that the electrocyclization reaction was sensitive to elevated temperatures, wherein isomeric products were formed. While similar Rh-catalysed electrocyclizations have been highly diastereoselective when existing stereocenters are within the heterocycle formed,[43,44] this application exhibited high diastereoselectivity with the distal acetonide stereocenters. To rationalize this finding, the 6π electrocyclization was computationally investigated.

DFT calculations executed at the ωB97x-D/6-31+G(d,p) level of theory map reaction progress from model substrate **44A** (Scheme 7B). The reaction pathway proceeds *via* this reactive s-*cis* azatriene (ΔG = +4.3 kcal mol^{-1} relative to the more stable s-*trans* conformer), which undergoes the 6π electrocyclization

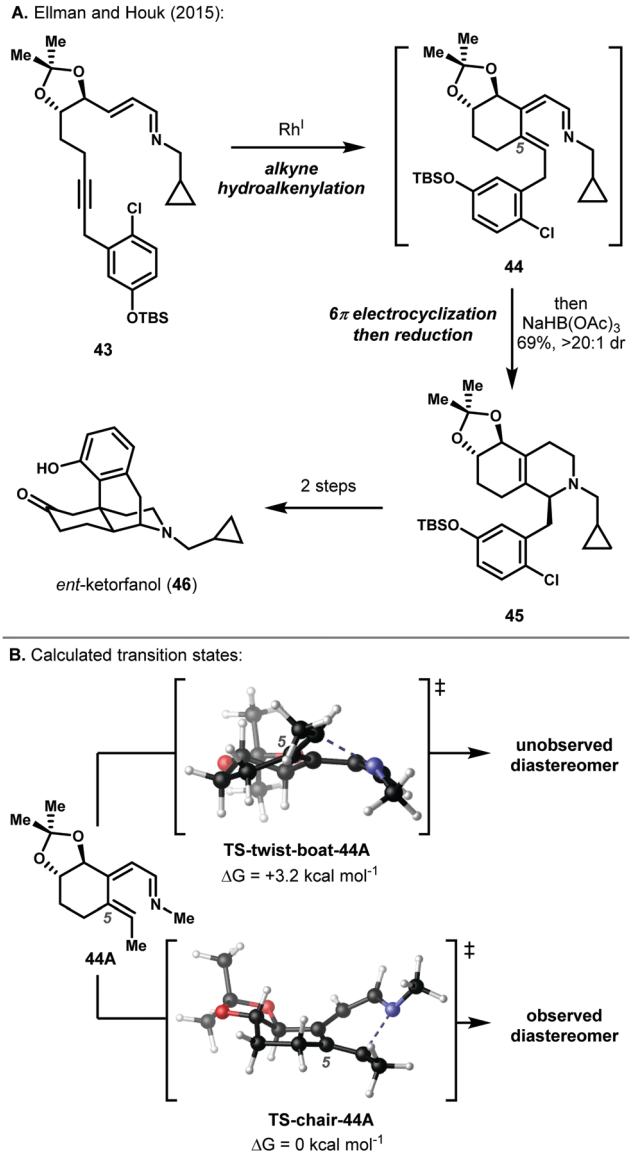

Scheme 7 (A) Synthesis of *ent*-ketorfanol (**46**). (B) Reaction pathways leading to diastereomeric products, with relative transition state energies.

through two distinct pathways. In the lower energy pathway, the existing cyclohexene core structure assumes a chair-like conformation, while in the higher energy pathway it distorts to a twist-boat cyclohexene configuration. This twist-boat ground state conformer is 3.8 kcal mol^{-1} higher in energy than the chair conformer. Both conformers proceed through 6-membered transition states to form diastereomeric products, with geometric constraints imposed by the cyclohexyl core structure. Consistent with the large energy differential in these systems, the diastereomeric product resulting from this twist-boat intermediate was not observed experimentally.

The energetic preference for the desired pathway is apparent in the transition states as well as the ground state structures. Modelling formation of the desired and undesired diastereomers, it emerged that the electrocyclization causes transient pyramidalization of C5 in the cyclohexene core structure of **44A**. In the favoured mode of cyclization, this atom is pushed downwards, enforcing the chair-like transition state ($\Delta G^{\ddagger}$ = +19.6 kcal mol^{-1}, **TS-chair-44A**), whereas the undesired mode of cyclization causes the twist-boat geometry to be reinforced by the upwards motion of C5 ($\Delta G^{\ddagger}$ = +22.8 kcal mol^{-1}, **TS-twist-boat-44A**). These forces are analogous to those influencing diastereoselectivity in the electrophilic functionalization of cyclohexenes,[45] supporting the formation of products intercepted by a chair-like transition state. The observed mode of cyclization was predicted to be kinetically favourable for various substitution patterns at nitrogen, the alkene, and the acetonide, by 3.1–3.6 kcal mol^{-1} for analogs of model substrate **44A**. With both kinetic and thermodynamic preference for one diastereomer, the high torquoselectivity of the reaction is imminently reasonable, even though the existing stereocenters are distal from the site of bond formation.

Cyclic conformational analysis is important in many transition and ground state structures and often has meaningful consequences for reaction outcomes. Careful attention to these factors enables product prediction and rationalization. This approach is supported by computational studies, whose visualizations and energy outputs offer insights in reactive systems. Such analysis is especially appropriate because of the relatively constrained transition state in this system. Caution as to truncation of substituents must be maintained lest steric interactions be inaccurately represented; that the authors observe similar predicted trends for a variety of substrate models supports the conclusions of their computational study. The preference for chair-like transition states are evident in electrocyclizations as well as electrophilic cyclohexene additions and other transformations.

3.2. Modelling diastereoselective intermolecular transformations: application to biosynthetic studies

Computational chemistry can be used to inform biosynthetic hypotheses,[11] as direct observation of compound assembly *in vivo* is often intractable. A biomimetic synthesis of the racemic natural product santalin Y (**51**, Scheme 8A) was reported by the laboratories of Trauner and Tantillo in 2015 that used experimental and theoretical methods to provide intriguing comments on the biosynthesis of the natural product.[46] The authors propose a biosynthetic pathway consisting of a concerted (3+2) cycloaddition of arenes **47** and **49** to form santalin Y (**51**). The cascade begins with proton transfer of **47** to form 1,3-dipole **48**, which undergoes a diastereoselective (3+2) cycloaddition with **49** to form **50**, followed by an intramolecular Friedel–Crafts reaction to complete the natural product.

At the bench, the authors assembled **47** and **49** and investigated abiotic reaction conditions to recapitulate the putative biosynthetic transformation. They found that triethylamine promoted the tandem proton transfer, cycloaddition, and Friedel–Crafts transformations to form santalin Y (**51**) in 67% yield. The success of this sequence and the complete selectivity for the natural diastereomer support the authors' biosynthetic hypothesis. To rationalize this selectivity and provide insights into the reaction mechanism, the authors performed a quantum mechanical analysis of the system.

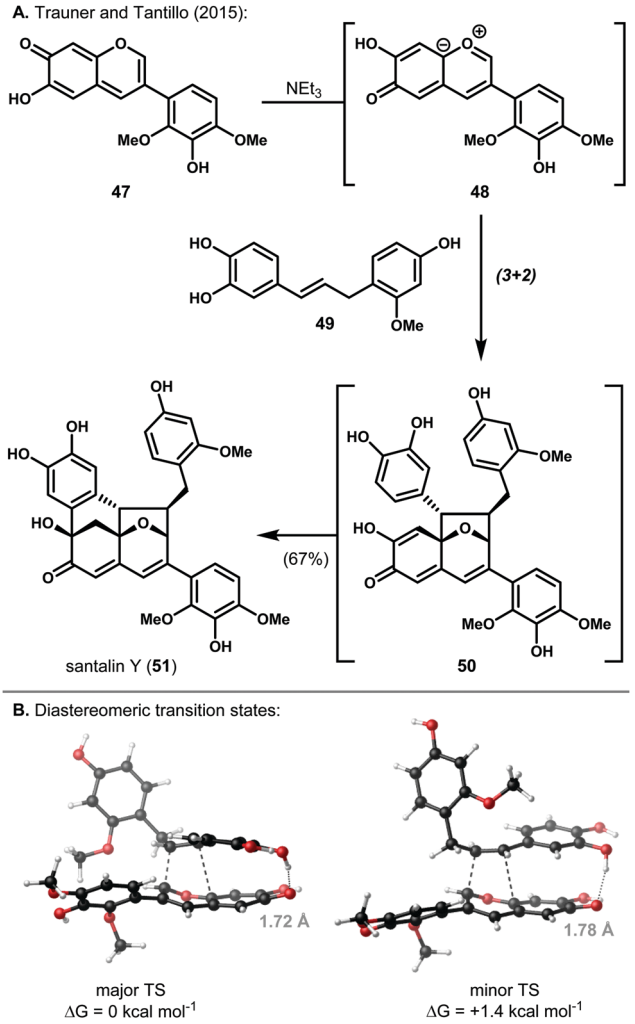

Scheme 8 (A) Biomimetic synthesis of santalin Y (**51**). (B) Computed transition states and energies leading to diastereomeric adducts.

To locate relevant structures, MMFF energy-minimized conformers were generated and ranked, with the top 100 subjected to DFT structure optimization and single point energy calculations. The authors investigated a number of levels of theory, with M06-2X/6-31G(d) results reproduced here. The proton transfer of **47** is kinetically and thermodynamically reasonable, with an activation barrier of +10.1 kcal mol^{-1} to form **48**, which is 9.6 kcal mol^{-1} higher in energy than **47**. The (3+2) cycloaddition was found to be kinetically accessible for both diastereomers, with the desired pathway favoured by 1.4 kcal mol^{-1} (Scheme 8B). Both transition states are characterized by hydrogen-bonding and π-stacking interactions at the catechol moieties. The hydrogen-bonding distance is slightly shorter in the major TS (1.72 Å as compared to 1.78 Å for the minor TS). The forming bond lengths are also slightly shorter in the favoured transition state, suggesting a later transition state for the pathway leading to the observed product. Subtle steric and electronic effects are responsible for these observations and preferentially stabilize the transition state leading to the observed diastereomer. The innate preference for the natural diastereomer supports the (3+2) cycloaddition as the biosynthetic origin of **51**. This is in contrast to the stepwise cyclization mechanism previously suggested for these metabolites,[47] which the authors were unable to affect experimentally. In addition, the authors could not computationally locate the intermediates associated with a stepwise transformation, further supporting a concerted cycloaddition pathway.

This synthetic and computational study supports detailed biosynthetic investigations of this cycloaddition process. The cycloaddition may occur in a biological context thermally or in the presence of a catalyst, such as an enzyme or other chemical agent. The experimental and theoretical feasibility of recapitulating the putative biosynthesis suggests that this reactivity is innately favourable and thus a similar transformation may occur in nature. Calculations that map biosynthetic transformations can support potential mechanisms, although the difficulty of accurately modelling biological conditions and enzyme active sites are worth mentioning.

This work provides a detailed molecular analysis for the factors that may influence the diastereoselectivity of a cycloaddition reaction. These subtle factors are not immediately evident using a qualitative analysis and calculations are poised to identify such preferences, with minute steric and electronic effects accounted for only by complex models and not by qualitative analysis.

3.3. Modelling enantioselectivity with computational chemistry: application to methods development

The intersection of total synthesis, methods development, and computational evaluation is showcased in the striking 2017 synthesis of himalensine A (**56**) by the groups of Dixon and Paton.[48] A key step in the synthesis involved an enantioselective intramolecular furan Diels–Alder reaction to furnish the 5,6,7-tricyclic core structure (**55**, Scheme 9A). The Diels–Alder precursor **52** was assembled from commercial materials, and after screening organocatalysts, the Diels–Alder reaction was optimized to an impressive 86% yield, 92 : 8 dr, and 90% ee. A bifunctional iminophosphorane (BIMP) superbase catalyst (**53**) was found to be superior to cinchona alkaloids or 1,4-diazabicyclo[2.2.2]octane (DABCO) for this transformation, enabling the elaboration of **55** to himalensine A (**56**). As a crucial asymmetric and annulative component of the synthetic route, the intramolecular furan Diels–Alder was modelled to account for the high diastereo- and enantioselectivity.

The authors used a range of DFT methods to assess the reaction profile, including energy minimization of substrate-catalyst complexes (M06-2X/def2-TZVP(SMD = PhMe)//M06-2X/def2-SVP, Boc modelled as CO_2Me), ^{1}H and ^{13}C NMR structure prediction of diastereomers (mPW1PW91/6-311+G(2d,p)),[8] and non-covalent interaction index isosurface analysis of reaction transition states (M06-2X).[49] The Diels–Alder transformation occurs after base-mediated α-deprotonation of **52A** forms extended enolate **58** and γ-protonation completes the 1,3-proton transfer to reveal dienophile **54A** (Scheme 9B). Modelling the DABCO-catalysed pathway predicted a rate-determining α-deprotonation where $\Delta G^{\ddagger}$ = +24.2 kcal mol^{-1}. By contrast, the BIMP-catalysed

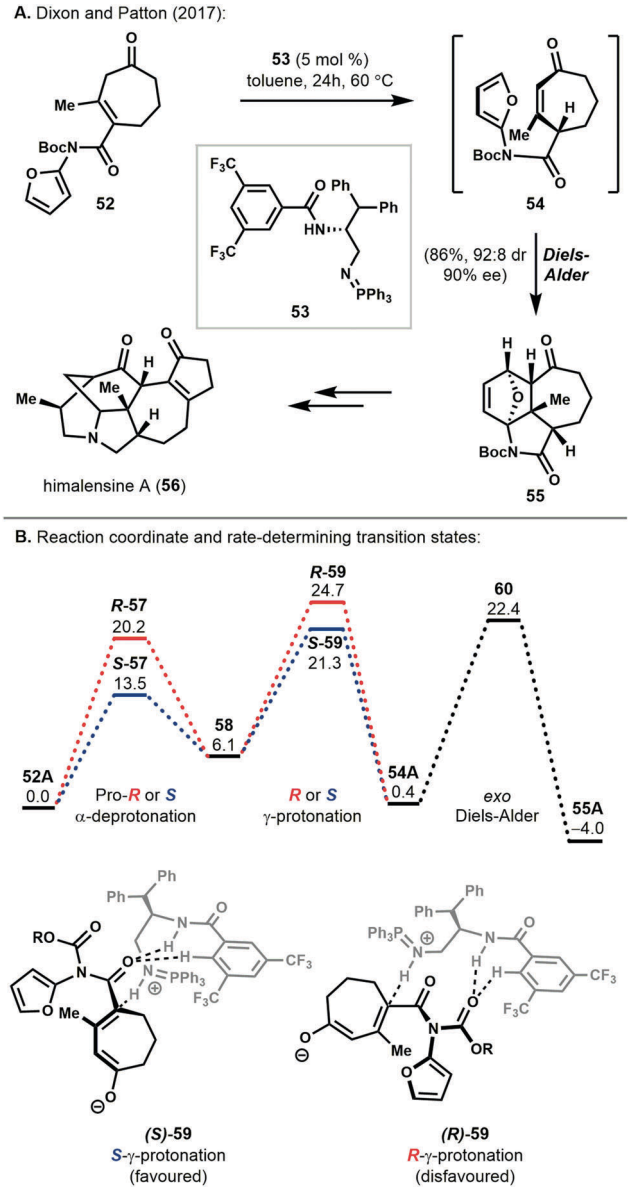

Scheme 9 (A) Synthesis of himalensine A (**56**) by an intramolecular furan Diels–Alder reaction. (B) Reaction coordinate with free energies in kcal mol^{-1}, and consequential transition state structures.

pathways are significantly lower in energy, highlighting the importance of non-covalent secondary interactions in catalysis.[50] In the BIMP pathway, both α-deprotonation (**57**) and γ-protonation (**59**) have transition states that favour the (*S*)-enantiomer. The γ-protonation is stereo-determining, and the energy difference between (*R*)-**59** and (*S*)-**59** predicted reaction enantiomeric excesses that were in close agreement with observed values.

Asymmetric induction is facilitated by hydrogen bonding between the catalyst and substrate. In the lower-energy transition state (*S*)-**59**, H-bonding takes place between both the catalyst amide and aryl H-donors, and the substrate amide carbonyl to deliver the γ-proton. In the higher-energy transition state (*R*)-**59**, the same H-donors engage the carbamate carbonyl instead, leading to less favourable H-bond interactions evidenced by greater distance between contacts. Furthermore, the minor pathway also features a steric interaction between the substrate methyl group and a catalyst aryl trifluoromethyl group. These structural observations explain the observed enantioselectivity.

The furan Diels–Alder then proceeds with high *exo*-selectivity due to the 11.6 kcal mol^{-1} greater stability of the *exo* transition state (**60**) relative to the *endo* transition state. The *exo* transition state is also significantly later in the reaction coordinate than the *endo* transition state, which is consistent with the greater stability of the *exo* adduct in the bond formation event. Analysis of the non-covalent interaction index isosurface implicates steric interactions around the quaternary methyl group and between the cyclohexene olefin and cycloheptanone ring in the *endo* product that are absent in the *exo* adduct **55**. Additionally, there is more transannular strain at the 6,7-ring fusion in the *endo* product, leading to a ground-state structure that is 19.0 kcal mol^{-1} less stable than the *exo* adduct. Within the *exo* pathway, there exist two possible diastereomers at the lactam α-position due to the conformational flexibility of the 7-membered ring. By modelling both *exo* products and transition states the authors predicted a product distribution of 97 : 3 at 60 °C, which agrees very well with the observed ratio of 96 : 4.

In addition to the use of calculations to inform synthetic studies, their application to the development of synthetic methodology is well recognized.[9,10] This example demonstrates that these approaches need not be separate, and that a detailed study of one transformation greatly complements a substantive synthetic effort. While catalytic cycles are often difficult to model because of complex mechanistic possibilities,[33] the authors' careful consideration of potential reaction pathways and thorough use of computational methods presents a highly responsible computational study. This work also highlights an explanation of enantioselectivity in concert with diastereoselectivity and reactivity, and the synergistic use of ground state and transition state structures to model substrates, products, and catalyst complexes.

4. Decoupling stabilizing interactions with computational model systems

The inexplicable instability of a target natural product often confounds synthetic researchers; calculations can rationalize this phenomenon and contribute to a broader understanding of stabilizing forces. One inspiring study was reported by Joullié and co-workers in their 2008 synthesis of roquefortine C (**63**, Scheme 10A).[51] Previous attempts to access this natural product were plagued by the competitive formation of the more stable isoroquefortine C (**64**).[52] Beginning with a tryptophan derivative (**61**), the authors assembled the pyrroloindoline tricyclic core and appended a dehydrohistadine moiety to form **62**, which underwent global deprotection and cyclization with tetramethylsilyl iodide and ammonia/methanol to form roquefortine C (**63**). Roquefortine C (**63**) was found to isomerize to isoroquefortine C (**64**) easily under acidic, basic, or photolytic conditions.[51,52] With the synthesis complete, the authors

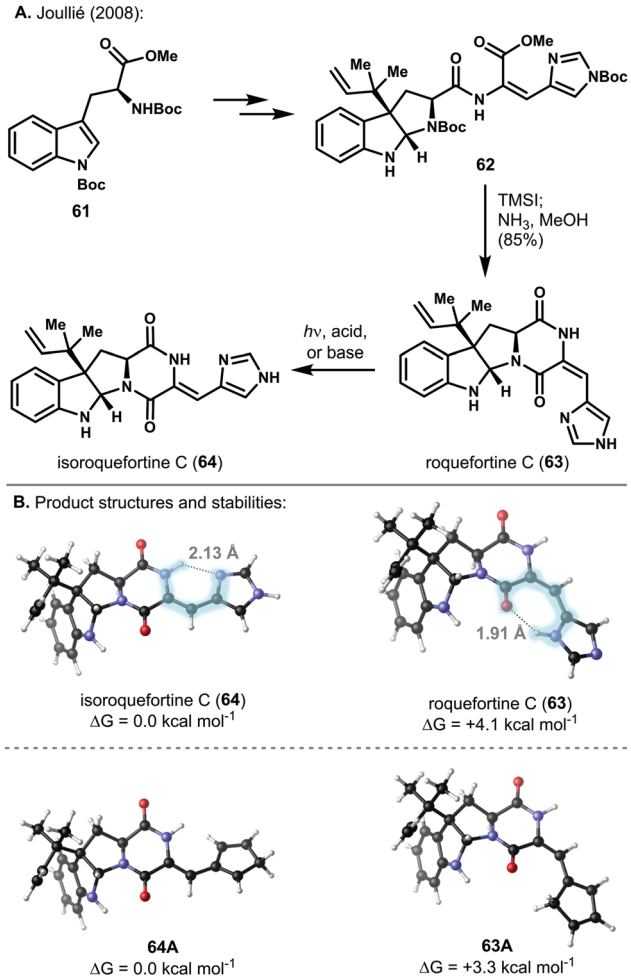

Scheme 10 (A) Synthesis of roquefortine C (**63**). (B) Calculated structures of natural products and analogs with relative energies.

investigated the reason for the thermodynamic preference for isoroquefortine C (**64**) using computational methods.

Molecular mechanics, Hartree–Fock (HF), and T1 methods were used to model **63** and **64** (Scheme 10B),[53] with HF results reproduced here. The authors found that isoroquefortine C (**64**) is more stable than the natural isomer by 4.1 kcal mol^{-1} and that the barrier to interconversion, which requires breaking conjugation of the π system, is +4.1–5.5 kcal mol^{-1} depending on the substrate. Both isomers possess a hydrogen bond between the imidazole and 2,5-diketopiperazine. In roquefortine C (**63**, tautomeric structure), the hydrogen bond distance is 1.91 Å while in isoroquefortine C (64) this distance is 2.13 Å. This would suggest a greater stability for roquefortine C (63),[54] but the opposite trend was calculated and observed. The authors hypothesized that hydrogen bonding does not significantly influence relative stability, and they evaluated analogs to test this hypothesis.

The authors modelled cyclopentadiene analogs of the histadines, **63A** and **64A**. These analogs cannot participate in hydrogen bonding but serve as isosteres for the heteroarenes in the real system.[55] It was found that the cyclopentadiene analog **64A** is 3.3 kcal mol^{-1} more stable than **63A**. This is the majority of the energy difference between the imidazole-containing natural products. The purported reason for this lies in the geometric constraints imposed by the planarity of the conjugated system. The planarity results from the abundance of sp^2 atoms; the ideal bond angle for these substituents is 120°, which is achieved by a six-membered ring configuration. In roquefortine C (**63**) there is a seven-membered ring configuration of sp^2 carbons in the hydrogen-bonded system, the greatest angle of which is 134° (blue highlight). By contrast, isoroquefortine C (**64**) contains a six-membered hydrogen-bonded ring of sp^2 atoms, for which the largest angle is 127° (blue highlight). This is much closer to ideality and explains the greater stability of **64** relative to **63**. This stability is maintained in the cyclopentadienyl analogs, despite introducing a sp^3-hybridized carbon in the ring system, because the ring-like conformation and planarity remains largely conserved.

In these studies, Joullié and co-workers explain the difference in stability between *E*/*Z* isomers **63** and **64** that convoluted the synthesis of natural product **63**. A hydrogen-bonding explanation did not account for the energetic difference between the structures. A hypothesis that implicated torsional strain and deviation from ideal bond angles as destabilizing factors was more consistent with predictions. The complex factors that influence stability were disentangled by judicious use of calculations on the real system and an analog system.

Model systems can be used to isolate factors such as electron density, hydrogen-bonding capability, and steric bulk that are hypothesized to influence calculated energies. In addition, computational techniques such as natural bond order and non-covalent interaction analyses can be used to identify and quantify specific atomic and molecular interactions. These computational experiments, especially when validated by empirical input, are powerful tools for understanding underlying chemical phenomena. This is especially advantageous when synthetic access to desirable analogs is not readily available.

5. Conclusions and outlook

This review has described how computational chemistry has assisted in understanding the reactivity of the intricate molecular architectures encountered in natural product synthesis. Numerous different types of calculations can now be performed to explain complicated reaction outcomes: lowest energy ground state conformations work in concert with *a priori* analysis, transition state calculations can differentiate enantiomeric and diastereomeric outcomes, and relative energies of reactive intermediates can approximate complex reaction pathways.

These methods can be applied to elucidate underlying chemical forces, predict reaction outcomes, and design more reactive systems. For each situation, the type of method (MM, quantum mechanical, semi-empirical) must be carefully chosen to complement the system of study and the requirements and resources of the practitioners. All computational methods make different approximations to model atomic interactions; understanding these assumptions and limitations is important for their responsible application. Generally speaking,

more accurate methods consume more computational resources, however continued technological and methodological advances have made performing complex calculations accessible to an increasingly general audience. The continuing adoption of computational chemistry and novel strategies for its application to complex molecule synthesis are expected to drive natural product synthesis to unprecedented levels of efficiency and heighten our fundamental understanding of chemical reactivity.

Conflicts of interest

There are no conflicts to declare.

Acknowledgements

This work was supported by Yale University, the Sloan Foundation, and a Dox Fellowship (M. E.).

Notes and references

1 J. C. Sheehan, *The Enchanted Ring: The Untold Story of Penicillin*, The MIT Press, Cambridge, Massachusetts, 1982.
2 K. C. Nicolaou and E. J. Sorensen, *Classics in Total Synthesis: Targets, Strategies, Methods*, VCH, New York, 1996.
3 F. R. Ornellas, *Theor. Chem. Acc.*, 2012, **131**, 1086.
4 Q. N. N. Nguyen and D. J. Tantillo, *Chem. – Asian J.*, 2014, **9**, 674–680.
5 T. Sperger, I. A. Sanhueza and F. Schoenebeck, *Acc. Chem. Res.*, 2016, **49**, 1311–1319.
6 K. Jackson, S. K. Jaffar and R. S. Paton, *Annu. Rep. Prog. Chem., Sect. B: Org. Chem.*, 2013, **109**, 235–255.
7 G.-J. Cheng, X. Zhang, L. W. Chung, L. Xu and Y.-D. Wu, *J. Am. Chem. Soc.*, 2015, **137**, 1706–1725.
8 M. W. Lodewyk, M. R. Siebert and D. J. Tantillo, *Chem. Rev.*, 2012, **112**, 1839–1862.
9 S. Niu and M. B. Hall, *Chem. Rev.*, 2000, **100**, 353–405.
10 N. Fey, *Dalton Trans.*, 2010, **39**, 296–310.
11 D. J. Tantillo, *Nat. Prod. Rep.*, 2011, **28**, 1035–1053.
12 R. Lonsdale and R. A. Ward, *Chem. Soc. Rev.*, 2018, **47**, 3816–3830.
13 M. H. Todd, *Chem. Soc. Rev.*, 2005, **34**, 247–266.
14 S. Szymkuć, E. P. Gajewska, T. Klucznik, K. Molga, P. Dittwald, M. Startek, M. Bajczyk and B. A. Grzybowski, *Angew. Chem., Int. Ed.*, 2016, **55**, 5904–5937.
15 C. W. Coley, W. H. Green and K. F. Jensen, *Acc. Chem. Res.*, 2018, **51**, 1281–1289.
16 W. C. Still, *J. Am. Chem. Soc.*, 1979, **101**, 2493–2495.
17 T. Takahashi, Y. Kanda, H. Nemoto, K. Kitamura, J. Tsuji and Y. Fukazawa, *J. Am. Chem. Soc.*, 1986, **51**, 3394–3396.
18 W. C. Still and I. Galynker, *Tetrahedron*, 1981, **37**, 3981–3996.
19 M. J. Kim, T.-i. Sohn, D. Kim and R. S. Paton, *J. Am. Chem. Soc.*, 2012, **134**, 20178–20188.
20 W. Jeong, M. J. Kim, H. Kim, S. Kim, D. Kim and K. J. Shin, *Angew. Chem., Int. Ed.*, 2010, **49**, 752–756.
21 S. Wolfe, *Acc. Chem. Res.*, 1972, **5**, 102–111.
22 D. A. Evans, D. J. Adams and E. E. Kwan, *J. Am. Chem. Soc.*, 2012, **134**, 8162–8170.
23 S. Bahmanyar and K. N. Houk, *J. Am. Chem. Soc.*, 2001, **123**, 11273–11283.
24 M. I. Page and W. P. Jencks, *Proc. Natl. Acad. Sci. U. S. A.*, 1971, **68**, 1678–1683.
25 C. J. Cramer and D. G. Truhlar, *Chem. Rev.*, 1999, **99**, 2161–2200.
26 J. Zhang, H. Zhang, T. Wu, Q. Wang and D. van der Spoel, *J. Chem. Theory Comput.*, 2017, **13**, 1034–1043.
27 J. W. Beatty and C. R. Stephenson, *J. Am. Chem. Soc.*, 2014, **136**, 10270–10273.
28 J. Schreiber and A. Eschenmoser, *Helv. Chim. Acta*, 1955, **38**, 1529–1536.
29 J. F. Liebman and A. Greenberg, *Chem. Rev.*, 1976, **76**, 311–365.
30 B. M. Trost, *Top. Curr. Chem.*, 1986, **133**, 3–82.
31 T. Dudev and C. Lim, *J. Am. Chem. Soc.*, 1998, **120**, 4450–4458.
32 G. A. Arteca and P. G. Mezey, *J. Comput. Chem.*, 1988, **9**, 728–744.
33 Y.-h. Lam, M. N. Grayson, M. C. Holland, A. Simon and K. N. Houk, *Acc. Chem. Res.*, 2016, **49**, 750–762.
34 H. Kruse, L. Goerigk and S. Grimme, *J. Org. Chem.*, 2012, **77**, 10824–10834.
35 J. P. Wagner and P. R. Schreiner, *Angew. Chem., Int. Ed.*, 2015, **54**, 12274–12296.
36 D. Balcells, E. Clot and O. Eisenstein, *Chem. Rev.*, 2010, **110**, 749–823.
37 N. C. Wilde, M. Isomura, A. Mendoza and P. S. Baran, *J. Am. Chem. Soc.*, 2014, **136**, 4909–4912.
38 R. Harnisch, G. Lauterbach and W. Pritzkow, *J. Prakt. Chem.*, 1995, **337**, 60–62.
39 K. C. Nicolaou, P. G. Nantermet, H. Ueno, R. K. Guy, E. A. Couladouros and E. J. Sorensen, *J. Am. Chem. Soc.*, 1995, **117**, 624–633.
40 T. R. Newhouse and P. S. Baran, *Angew. Chem., Int. Ed.*, 2011, **50**, 3362–3374.
41 D. J. Tao, Y. Slutskyy, M. Muuronen, A. Le, P. Kohler and L. E. Overman, *J. Am. Chem. Soc.*, 2018, **140**, 3091–3102.
42 Q. Peng, F. Duarte and R. S. Paton, *Chem. Soc. Rev.*, 2016, **45**, 6093–6107.
43 E. M. Phillips, T. Mesganaw, A. Patel, S. Duttwyler, B. Q. Mercado, K. N. Houk and J. A. Ellman, *Angew. Chem., Int. Ed.*, 2015, **54**, 12044–12048.
44 S. Tompson, A. G. Coyne, P. C. Knipe and M. D. Smith, *Chem. Soc. Rev.*, 2011, **40**, 4217–4231.
45 A. Furst and P. Plattner, *Helv. Chim. Acta*, 1949, **32**, 275–283.
46 S. Strych, G. Journot, R. P. Pemberton, S. C. Wang, D. J. Tantillo and D. Trauner, *Angew. Chem., Int. Ed.*, 2015, **54**, 5079–5083.
47 J. Kinjo, H. Uemura, T. Nohara, M. Yamashita, N. Marubayashi and K. Yoshihira, *Tetrahedron Lett.*, 1995, **36**, 5599–5602.
48 H. Shi, I. N. Michaelides, B. Darses, P. Jakubec, Q. N. N. Nguyen, R. S. Paton and D. J. Dixon, *J. Am. Chem. Soc.*, 2017, **139**, 17755–17758.

49 E. R. Johnson, S. Keinan, P. Mori-Sánchez, J. Contreras-Garcia, A. J. Cohen and W. Yang, *J. Am. Chem. Soc.*, 2010, **132**, 6498–6506.
50 H. J. Davis and R. J. Phipps, *Chem. Soc. Rev.*, 2017, **8**, 864–877.
51 N. Shangguan, W. J. Hehre, W. S. Ohlinger, M. P. Beavers and M. M. Joullié, *J. Am. Chem. Soc.*, 2008, **130**, 6281–6287.
52 D. J. Richard, B. Schiavi and M. M. Joullié, *Proc. Natl. Acad. Sci. U. S. A.*, 2004, **101**, 11971–11976.
53 W. S. Ohlinger, P. E. Klunzinger, B. J. Deppmeier and W. J. Hehre, *J. Phys. Chem. A*, 2009, **113**, 2165–2175.
54 M. S. Gordon and J. H. Jensen, *Acc. Chem. Res.*, 1996, **29**, 536–543.
55 G. A Patani and E. J. LaVoie, *Chem. Rev.*, 1996, **96**, 3147–3176.